Towards the valorization of Cumbre Vieja volcanic ash – Production of alternative cements

M.M. Tashima , L. Soriano, M.V. Borrachero, J. Monzó, J. Payá [*]

Grupo de Investigación en Química de los Materiales (GIQUIMA), Instituto de Ciencia y Tecnología del Hormigón (ICITECH), Universitat Politècnica de València, Spain

ARTICLE INFO

ABSTRACT

One of the most critical issues after a volcanic eruption is managing damaged infrastructure and human health. This study aims to promote the valorization of non-weathered volcanic ash (VA) from the Cumbre Vieja volcano (La Palma Island – Spain) in the production of alternative cements. A detailed study related to the characterization of VA was performed, and its use in the production of alkali-activated cements is proposed. Promising results, achieving about 80 MPa in compression, indicated that using a cementing material based on VA could be a fascinating solution for the VA valorization and the reconstruction of the affected infrastructure of La Palma Island, especially in producing prefabricated elements.

1. Introduction

After 50 years of silence, the Cumbre Vieja volcano reawoke and devasted a wide area far beyond the vicinity. On September 19th 2021, the inhabitants of La Palma, the most north-westerly island of the Canary Islands – Spain, remained astonished by the beginning of the eruption of the Cumbre Vieja volcano (Fig. 1a). The volcano stayed active until December 13th 2021, it means 85 days – the most prolonged active-period on the island since historical records [1] (Fig. 1b). Indeed, this is the most significant episode reported for the Cumbre Vieja volcano since 1500 [2].

The eruptive episode damaged about 3000 buildings and approximately 74 km of roads: the infrastructure damage is calculated at 400 million euros [1,2]. Since the beginning, the explosive activity (yielding a maximum range of 1.5 km) associated with the effusive lava flows (up to 700 m/h) suggests that more than 200 million cubic meters of material erupted, reaching about 12 km^2 [1,3]. Many towns on the La Palma island were affected by the eruption, including both at the west of the island in the Llanos de Aridane and Tazacorte municipalities and, at the east of the island, in Villa de Mazo (where is located the airport).

According to experts, the extension of the affected area in an eruptive event depends on several factors, such as eruption duration, wind direction, and height of the plume [4]. Besides the damage caused by the lava flows, the scattered volcanic ash could be responsible for promoting contamination of aquifers due to the leaching of metals, human respiratory problems, serious infrastructure problems, and structural damage

to buildings due to its accumulation on roofs or reduced traction on roads or airports runways [5]. Taking into account the acquired experience of other eruptive events worldwide, the primary aspect of being solved is related to the reconstruction of the buildings for community relocation and the adequate disposal of erupted material such as volcanic ash (VA) [6]. The accumulation and collection of volcanic ash at La Palma island can be observed in the images shown in Fig. 2.

The possibility of valorization of volcanic ash as raw material in the production of construction materials could be a sustainable alternative to contribute to the reconstruction of damaged infrastructure and the management of disposed volcanic ash.

The first use of volcanic ash as construction material date back to the ancient Romans [7]. Due to its chemical composition and potential reactivity with Portland cement, the use of volcanic ashes is reported on European and American standards for cement manufacturing and use in concrete, respectively [8,9]. Moreover, several scientific papers reported the use of VA in mortars and concrete, recommending its maximum usage of 20 % replacing Portland cement due to the significant reduction in the mechanical properties compared to a reference sample [10].

In the last decades, alternative binding materials have been developed to reduce the environmental problems associated with Portland cement production and promote waste materials' valorization [11]. The alkali-activated cements are produced by a chemical reaction of an aluminosilicate material (precursor) with an alkaline activating solution (activator), forming an insoluble and durable binding compound named
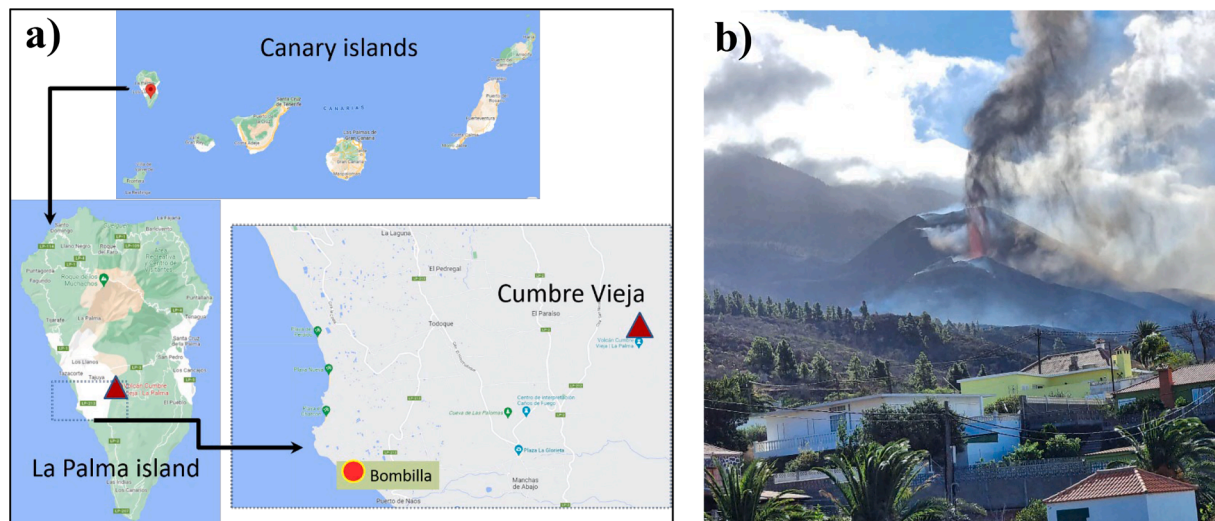
Fig. 1. Cumbre Vieja volcano: a) location on La Palma island (Canary islands) and location of the sampling point (Bombilla town); b) image of eruption by November 2021.

Fig. 2. Accumulation and collection of volcanic ash in the municipalities close to the Cumbre Vieja volcano.
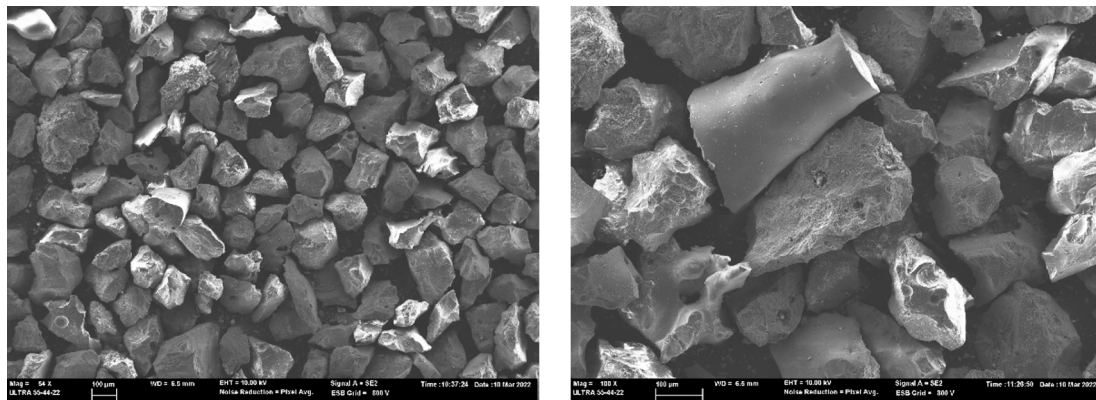

Fig. 3. FESEM micrographs of VA (sieved between 250 and 125 μm).

N-A—S—H gel [11]. In this case, the use of Portland cement is unnecessary, and a high volume of waste material can be valorized. Several studies report the use of different waste materials as precursors for alkali-activated cement, such as coal fly ash [12], ceramic wastes [13], and fluid catalytic cracking catalyst residue [14], among others. The use of VA as an aluminosilicate source is also reported, and, depending on its origin/composition, type/concentration of the alkaline activating solution, and curing conditions, compressive strength in the range of 17–60 MPa can be achieved using this alternative cement [10,15,16].

Above mentioned studies were performed using VA, as these ashes were submitted to weathering during the time. Weathering means physical, chemical, and biological actions that could promote diagenetic processes that modify the mineralogy and reactivity of VA [10]. According to the literature, different kinds of clay minerals can be formed due to the weathering of VA, such as: allophane, imogolite, halloysite, bentonite and illite [17–19].

Hence, besides promoting the correct management and valorization of volcanic ash, the main contribution of this study is to assess the possibility of using a non-weathered Cumbre Vieja volcanic ash in the production of alkali-activated cements.
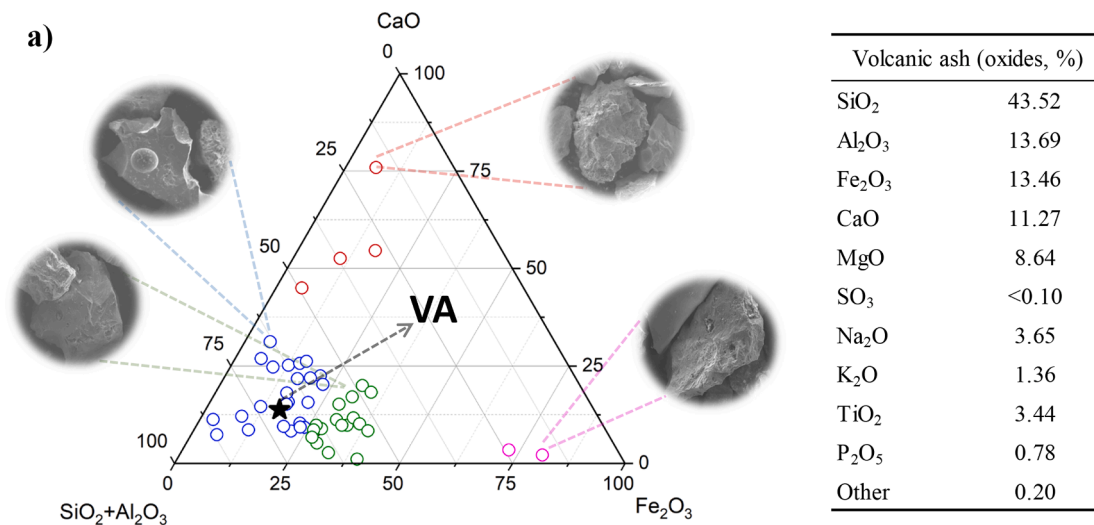
a)

Volcanic ash (oxides, %)	
SiO_2	43.52
Al_2O_3	13.69
Fe_2O_3	13.46
CaO	11.27
MgO	8.64
SO_3	<0.10
Na_2O	3.65
K_2O	1.36
TiO_2	3.44
P_2O_5	0.78
Other	0.20

Fig. 4. a) Ternary diagram ($SiO_2 + Al_2O_3$, Fe_2O_3, CaO) for as-received VA particles in the range 250–125 μm (determined by EDX); b) Chemical composition (wt.%) of VA sample, determined by XRF. Keys: green circles – particles containing relative Fe_2O_3 (25.0–37.5 wt%), $SiO_2 + Al_2O_3$ (50.0–70.0 wt%) and calcium oxide (0.0–25.0 wt%); blue circles – particles containing Fe_2O_3 (0.0–25.0 wt%), $SiO_2 + Al_2O_3$ (56.3–75.0 wt%) and calcium oxide (0.0–25.0 wt%); red circles – particles containing high relative CaO content (over 50 wt%); and purple circles – particles containing high relative Fe_2O_3 content (around 75.0 wt%). The symbol "star" represents the global chemical composition of VA in the ternary diagram. (For interpretation of the references to colour in this figure legend, the reader is referred to the web version of this article.)
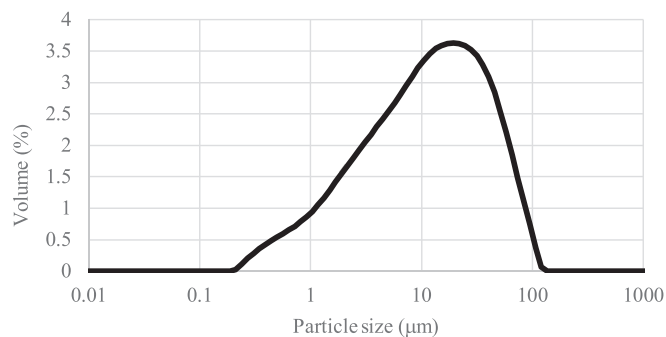

Fig. 5. Particle size distribution of Cumbre Vieja volcanic ash after the milling process.
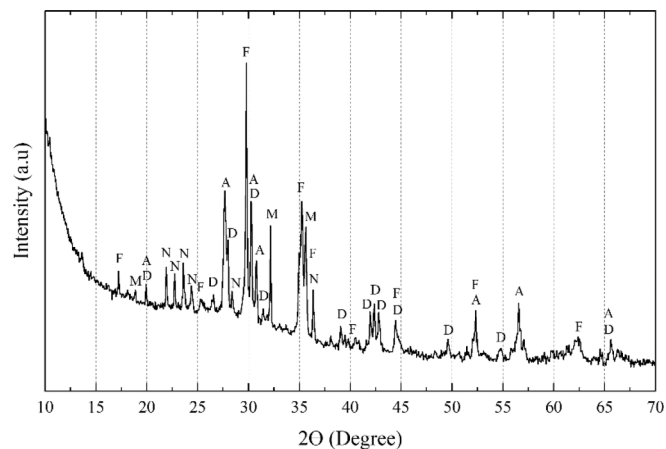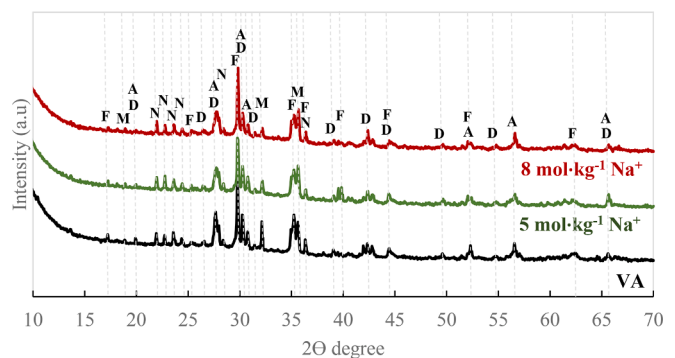

Fig. 7. XRD diffractograms for ground VA and alkali-activated pastes for 7 days at 65 °C using 5 and 8 mol·kg^{-1} of Na^+. Keys: F-forsterite (Mg_2SiO_4, pdfcard #040768); M-Maghemite (Fe_2O_3, pdfcard #251402); D-diopside ($CaMg(SiO_3)_2$, pdfcard #190239); A-Augite ($Ca(Mg,Fe)Si_2O_6$, pdfcard #240203); N-sodium-calcium anorthite ($(Ca,Na)(Si,Al)_4O_8$, pdfcard #181202).

2. Experimental program

2.1. Materials

NaOH pellets (98 % purity, from Panreac S.L.U), sodium silicate (8 % Na_2O, 28 % SiO_2, and 64 % H_2O, from Merck S.L.U) and tap water were used in the preparation of alkaline activating solutions. Cumbre Vieja volcanic ash from La Palma Island was used as a precursor in the production of alkali-activated cement. The in-situ collection of volcanic ash was performed by the Spanish Military Emergency Unit (UME) in the Bombilla municipality (La Palma island, Canary Islands, Spain). The material was sent to the Institute of Science and Technology of Concrete (ICITECH) at the Polytechnic University of Valencia – Spain.

2.2. Conditioning of VA

All the VA sample was dried in an oven at 100 °C before this use. On one hand, to characterize the morphological structure and the chemical composition of the as-received particles (sieved between 250 and 125 μm), a representative sample was obtained before the sieving process.

Fig. 6. XRD pattern of Cumbre Vieja volcanic ash. Keys: F-forsterite (Mg_2SiO_4, pdfcard #040768); M-Maghemite (Fe_2O_3, pdfcard #251402); D-diopside ($CaMg(SiO_3)_2$, pdfcard #190239); A-Augite ($Ca(Mg,Fe)Si_2O_6$, pdfcard #240203); N-sodium-calcium anorthite ($(Ca,Na)(Si,Al)_4O_8$, pdfcard #181202).
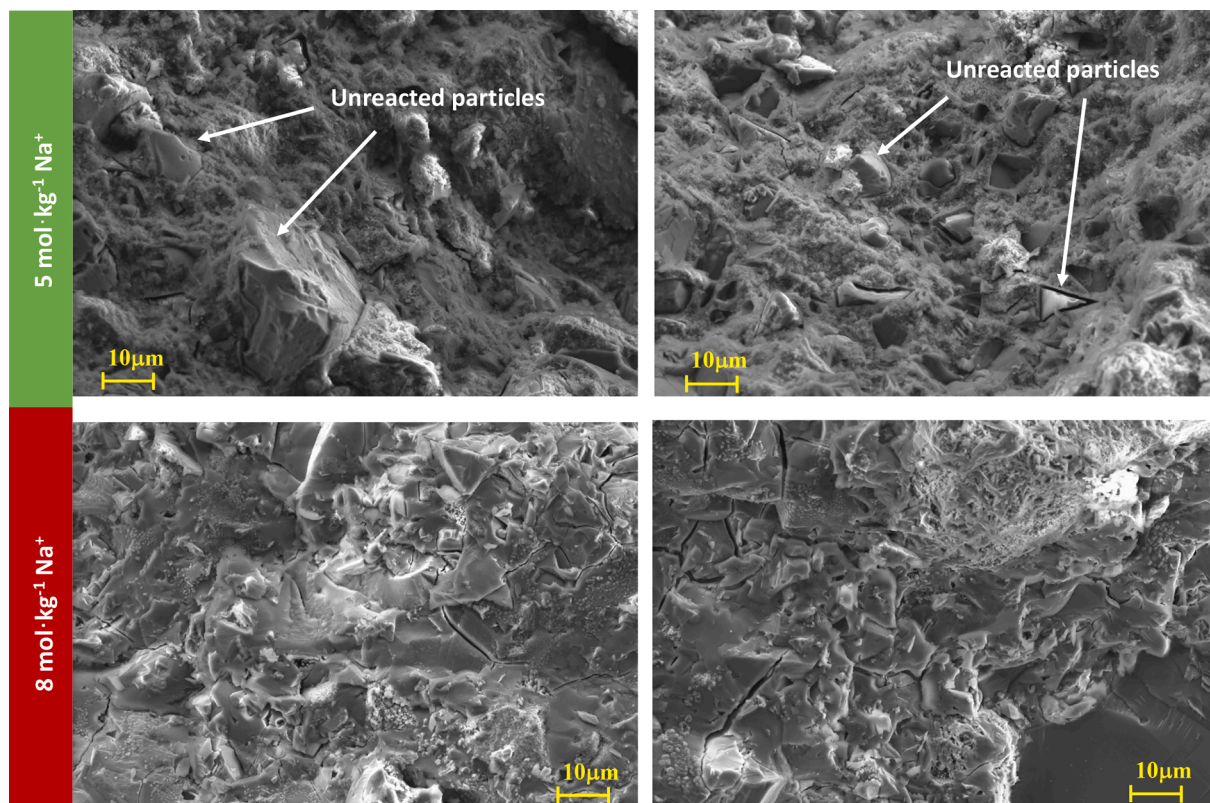
Fig. 8. FESEM micrographs of alkali-activated pastes cured at 65 °C for 7 days.

Table 1
EDX analysis of alkali-activated pastes cured at 65 °C for 7 days.

Oxides (%)	5 mol.kg^{-1} of Na$^+$			8 mol.kg^{-1} of Na$^+$		
	Mean (*)		Stand. Dev.	Mean (*)		Stand. Dev.
Na$_2$O	12.11	(7.19)	1.73	22.87	(9.30)	5.65
MgO	3.61	(7.83)	1.38	2.73	(7.34)	0.68
Al$_2$O$_3$	12.01	(12.41)	1.61	9.46	(11.65)	0.81
SiO$_2$	43.85	(44.92)	2.17	43.45	(45.76)	3.03
P$_2$O$_5$	1.72	(0.71)	1.73	0.56	(0.66)	0.30
K$_2$O	1.50	(1.24)	0.19	1.40	(1.16)	0.20
CaO	7.29	(10.22)	2.08	5.19	(9.58)	0.73
TiO$_2$	2.31	(3.12)	0.39	1.91	(2.93)	0.15
Fe$_2$O$_3$	15.59	(12.20)	3.64	12.43	(11.44)	1.89

*- Represent the theoretical chemical composition (oxides%) of alkali-activated paste considering the chemical composition of VA (Fig. 4b) and their respective alkaline activating solutions.

On the other hand, the VA sample was milled using a ball mill (Nannetti Speedy1) containing 65 alumina balls (20 mm of diameter). For each milling process, 600 g of VA were ground during 70 min.

2.3. Alkali-activated cements preparation

For the production of alkali-activated systems based on VA, an alkaline activating solution is necessary. This solution was prepared at least one hour before its use for cooling down the solution until room temperature. Tap water, NaOH, and Na$_2$SiO$_3$ are weighed separately and mixed in a beaker, which is covered with a plastic film to prevent evaporation from the heat of the reaction. The precursor was mixed with the alkaline activating solution using a mechanical stirrer for 4 min. The mixture was poured into metal molds for preparing prismatic 1*1*6 cm^3 samples. The molds were covered with a plastic bag to prevent evaporation and moisture losses and placed inside a plastic box in a thermostatic bath at 65 °C for 24 h. Once the first 24 h were completed, the

samples were demolded, and the specimens were kept in the plastic box in the thermostatic bath until the compressive strength test.

In a first step, the influence of curing temperature (45, 65 and 85 °C) for alkali-activated pastes activated with different Na$^+$ concentrations (5 and 8 mol·kg^{-1}) for a 1.46 SiO$_2$/Na$_2$O molar ratio (H$_2$O/Na$_2$O molar ratio of 22.2 and 13.9, respectively) and a constant H$_2$O/Na$_2$O mass ratio of 0.25 were evaluated. Finally, the effect of curing time (12, 24, 48, 72 and 168 h) at 65 °C was performed for a selected paste.

2.4. Tests performed

Mechanical, microstructural and nanostructural characterizations of VA and alkali-activated pastes were carried out. The morphological and the chemical composition was performed using a field emission scanning electron microscopy (FESEM – ULTRA 55 Zeiss Oxford instruments) containing an X-ray energy dispersive detector (EDX, Oxford Instruments) and working at 10 kV with a distance between 6 and 8 mm. The samples were covered with carbon using high vacuum coating equipment (BAL-TEC SCD 005). The particle size distribution and the granulometric parameters (mean particle diameter, d(0.9), d(0.5) and d(0.1)) of milled VA was determined using a laser diffraction granulometer (Mastersizer 2000 from Malvern Instruments). The chemical composition of VA sample was determined using X-ray fluorescence equipment (Philips Magic Pro Spectrometer). The mineralogy of VA and alkali-activated pastes were assessed by X-ray diffraction (Bruker AXS D8 Advance) from 10 to 70°, using Cu Kα radiation at 20 mA and 40 kV with a time accumulation of 2 s with a 0.02° angle step. The nanostructure transformation of alkali-activated pastes along the curing time was assessed by Fourier transform infrared spectroscopy using attenuated total reflection (FTIR-ATR) technique with spectra in the range 400–1200 cm^{-1} and a resolution of 2 cm^{-1} and 256 scans (Bruker Tensor 27). The compressive strength of the alkali-activated pastes was performed in a universal Instron Model 3382 machine with a maximum load of 100 kN.
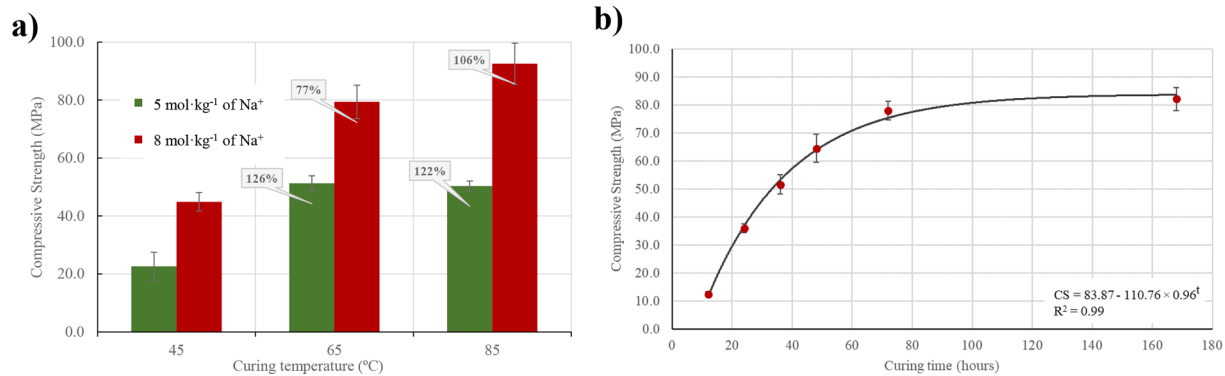
Fig. 9. Compressive strength of alkali-activated systems based on VA: a) Effect of curing temperature; b) Influence of curing time for pastes activated with 8 mol·kg^{-1} of Na$^+$ and cured at 65 °C. (Data label on Fig. 5a represents the compressive strength gain due to the increment of the curing temperature, with respect to the sample cured at 45 °C).

For all microstructural and nanostructural analyses, the reaction process was stopped by grinding the alkali-activated paste with acetone in an agate mortar, and then dried in an oven at 60 °C for 1 h. For FESEM analysis, fractured samples were employed.

3. Results and discussion

3.1. Characterization of Cumbre Vieja volcanic ash

Physico-chemical characterization of the Cumbre Vieja volcanic ash was performed using different instrumental techniques. A detailed study using FESEM/EDX micrographs was conducted for as-received particles (sieved between 250 and 125 μm) to assess their morphological structure and chemical composition, indicating the variety of type-particles (shape, angularity, density, porosity) (see Fig. 3).

Furthermore, over 50 EDX analyses were performed to assess the chemical composition of the as-received particles (sieved between 250 and 125 μm), and the obtained results were depicted as a ternary diagram (Fe$_2$O$_3$)–(CaO)–(SiO$_2$ + Al$_2$O$_3$) (Fig. 4a).

Most particles present high relative SiO$_2$ + Al$_2$O$_3$ content (in the range 50-75 wt%), about 10–25 % of calcium oxide, and 0.0–37.5 wt% of Fe$_2$O$_3$. These particles represent about 90 % of the assessed particles. Among these particles, about 60 % present a Fe$_2$O$_3$ content in the range 0.0–25.0 % wt. (represented as blue circles, Fig. 4a), while the other 40 % present higher relative Fe$_2$O$_3$ content (25.0–37.5 wt%) (defined as green circles, Fig. 4a). Besides the difference in the chemical composition, it is not very easy to visualize differences in the morphological structure of particles. On the other hand, the presence of minor amounts of particles containing a high percentage of calcium oxide (over 50 wt%) (red circles, Fig. 4a) and others having a high proportion of Fe$_2$O$_3$ (around 75 wt%) (purple circles, Fig. 5) were also detected. Comparing the morphological structure of these singular particles with respect to particles containing high relative SiO$_2$ + Al$_2$O$_3$, it was observed that they present a more porous structure (see detailed and comparative FESEM images in Fig. 4a).

An as-received sample was ground to valorize the VA in an alkali-activated binder, reducing its particle size and increasing its potential reactivity. The milled VA presents a mean particle diameter of 20.63 μm with the following percentiles: d(0.9), d(0.5), and d(0.1) of 52.26 μm, 12.56 μm, and 1.61 μm, respectively (determined by laser diffraction granulometry, see Fig. 5). FESEM images of milled VA show the presence of compact particles (which agrees with the high value of the VA density of 2.79 g/cm^3) with irregular shape.

The chemical composition of the VA sample, determined by X-ray fluorescence (XRF), is summarized in Fig. 4b. The sum of acidic oxides (SiO$_2$ + Al$_2$O$_3$ + Fe$_2$O$_3$) was 70.67 %, which is slightly higher than 70 %, the minimum chemical requirement for the use as natural pozzolan in concrete [9]. Another critical issue is the presence of CaO. It is well

known that materials containing high amounts of CaO in their composition, such as class C fly ash or blast furnace slag, can chemically react with water forming a binding material (hydraulic property). VA presented about 11.3 % of CaO; nevertheless, tests demonstrated that Cumbre Vieja VA does not present hydraulic property. The sulfur content in VA was negligible (%SO$_3$ < 0.1 %), which means that most of the sulfur emitted by the volcano was in the gas form, and the ash retained only a small part. Typically, the alkalis were present in a significant percentage, being the eq(Na$_2$O)% of 4.55 %. As was expected, the representation of VA on the ternary diagram is located in the zone of (represented by the "star" symbol in Fig. 2a) the particles containing Fe$_2$O$_3$ (0.0–25.0 wt%), SiO$_2$ + Al$_2$O$_3$ (56.3–75.0 wt%) and calcium oxide (0.0–25.0 wt%), it means "blue circles" in Fig. 4a.

Besides the characteristic oxides found in VA (SiO$_2$, Al$_2$O$_3$, CaO, and Fe$_2$O$_3$), other oxides, such as MgO, TiO$_2$, and Na$_2$O, could also be detected by XRF. These oxides are usually found on tephrite-basanite ashes, such as the ash erupted by the Cumbre Vieja volcano [2].

The XRD pattern of VA detected the presence of augite (Ca(Mg,Fe) Si$_2$O$_6$), diopside (CaMg(SiO$_3$)$_2$), sodium-calcium anorthite ((Ca,Na)(Si, Al)$_4$O$_8$), maghemite (Fe$_2$O$_3$) and forsterite (Mg$_2$SiO$_4$) (see Fig. 6). These minerals are usually found in volcanic ashes and, their presence in the ash depends on both eruption conditions and the magma configuration, nearly amorphous phase or completely crystalline structures can be formed [20]. Otherwise, a baseline deviation in the range 2$\ominus$ = 15–45°, indicative of the presence of amorphous phase, was also detected for Cumbre Vieja VA. Ndjock et al. and Djobo et al. [21,22] also reported the presence of an amorphous phase on VA collected from different deposits in Cameroon.

3.2. Effect of Na$^+$ concentration and curing temperature on alkali-activated systems

A comparative analysis between alkali-activated pastes activated with 5 and 8 mol.kgmol·kg^{-1} was performed. According to the XRD pattern of alkali-activated pastes after 7 curing days at 65 °C, the main crystalline phases of VA remain unchanged in the pastes (see Fig. 7). This behavior was also reported by Barone et al. [23] and Djobo et al. [15]. No differences in the XRD pattern were observed between pastes activated with 5 mol.kgmol·kg^{-1} and 8 mol.kgmol·kg^{-1} of Na$^+$. In the same way, no new crystalline phases (zeolitic phases) were observed for the alkali-activated pastes, indicating that the amorphous binding phase (N-A—S—H gel) does not transform in zeolitic phases. Even so, the high crystallinity of mineral phases present in VA hinders the visualization of baseline deviation in the range of 15–30°, typically found in alkali-activated systems [24].

The microstructure of alkali-activated binders was assessed using FESEM/EDX analyses. Fig. 8 shows the amorphous structure of the binder phase for both pastes activated with 5 mol·kg^{-1} and 8 mol·kg^{-1}
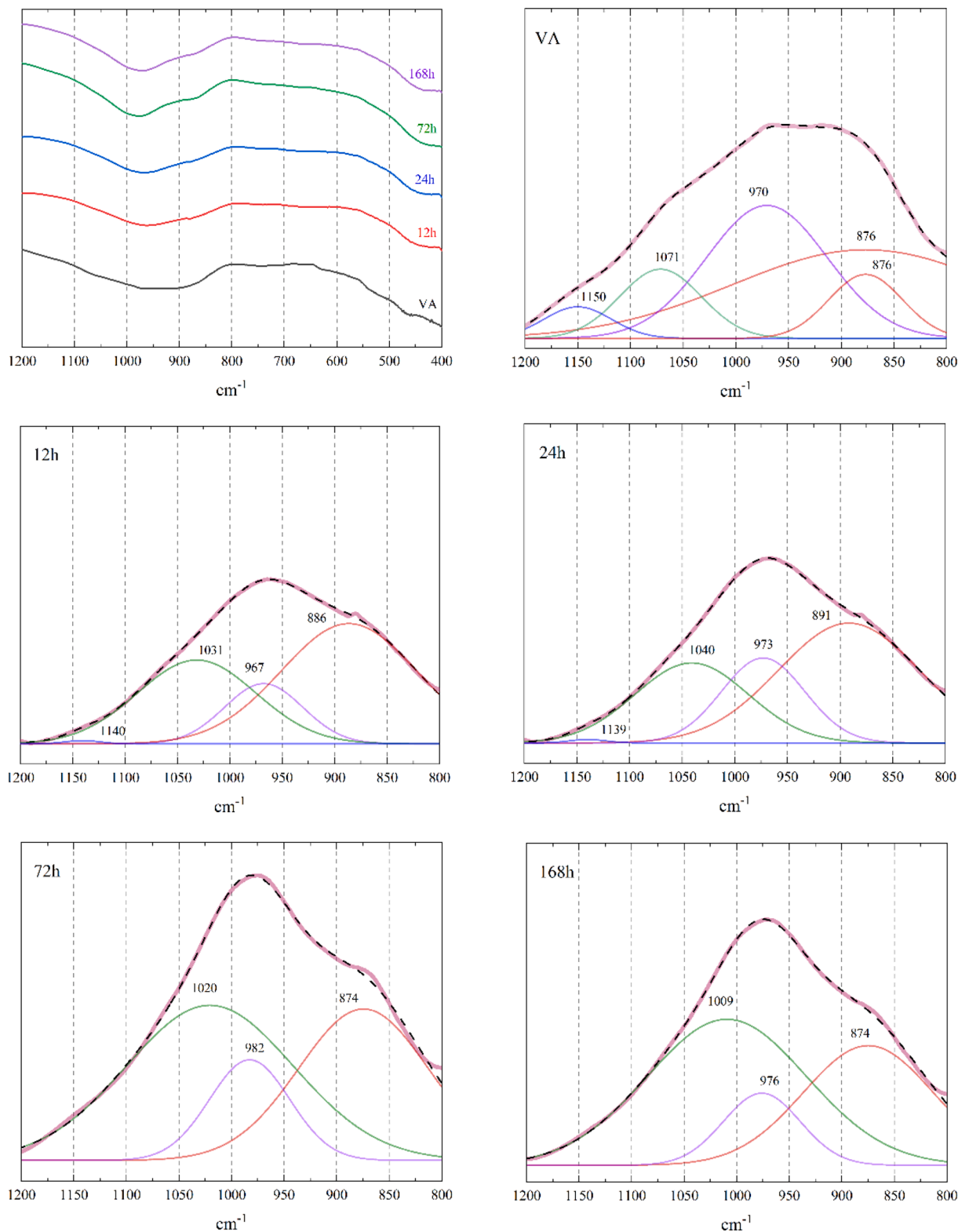
Fig. 10. FTIR-ATR results (1200–400 cm^{-1} range) obtained for VA and 8 mol·kg^{-1} paste cured for 12, 24, 72 and 168 h and the corresponding deconvolution curves for the 1200–800 cm^{-1} range.

of Na$^+$. The main two differences observed for alkali-activated paste activated with 8 mol·kg^{-1} with respect to the one with 5 mol·kg^{-1} are the denser and more compact structure and the reduced amount of unreacted volcanic ash particles with the corresponding increment on the N-A—S—H gel formation. Probably, it can lead to increments in the compressive strength of alkali-activated pastes.

Microanalysis was performed in both pastes using EDX, and the determined chemical composition of gel structure corresponds to N-A—S—H gel. Pastes activated with 8 mol·kg^{-1} of Na$^+$ presented a higher amount of sodium in the gel composition (see Table 1). In the same way, the presence of iron in the N-A—S—H gel structure was observed, probably replacing Al [25,26].

Table 2

The relative area from deconvolution FTIR-ATR bands with respect to VA for different curing times.

Band (cm^{-1})	Curing time (h)			
	12 h	24 h	72 h	168 h
891–874	0.961	0.934	0.673	0.646
982–967	0.500	0.698	0.495	0.411
1070–1009	2.948	2.524	4.436	4.805
1150–1139	0.093	0.092	–	–

Fig. 9**a** shows the effect of curing temperature on the compressive strength of alkali-activated pastes based on VA. An increment in the Na$^+$ concentration is associated with enhancement on the compressive strength, independently of the curing temperature. Specimens activated with 5 mol·kg^{-1} and cured at 45 °C yielded 22.6 MPa after 7 curing days, while 8 mol·kg^{-1} specimens achieved 44.9 MPa. It represents an enhancement of 98 % by just increasing the Na$^+$ concentration. The increment in alkali ions is responsible for the faster dissolution process of VA and, consequently, increases the formation of N-A—S—H gel binding phase [27]. Another critical issue is related to unreacted particles (mineral phases) of VA, which could act as nucleation points that favor the formation of N-A—S—H gel or even as microfiller, improving the mechanical strength of alkali-activated pastes [28]. This synergic effect could be responsible for the high compressive strength achieved by alkali-activated systems based on this VA. Several unreacted VA particles (see Fig. 8) are identified for pastes activated with 5 mol·kg^{-1} of Na$^+$.

Tashima et al. [29] also reported the effect of alkali concentration on the compressive strength of alkali-activated mortars based on vitreous calcium aluminosilicate. Mortars activated with 7.5 mol·kg^{-1} of Na$^+$ achieved a 31.4 % of increment with respect to mortars activated with 5 mol·kg^{-1} of Na$^+$. In the present study, for systems activated with 8 mol·kg^{-1}, there is a higher content of SiO$_2$, because the SiO$_2$/Na$_2$O molar ratio was maintained constant in the activator: this additional amount of reactive silicon-based compound (as silicate anion from sodium silicate reagent) produced a more considerable amount of N-A—S—H gel.

Moreover, the increment of curing temperature also represents an enhancement of the mechanical properties of alkali-activated systems. The data label in Fig. 9**a** illustrates the compressive strength gain due to the increment in the curing temperature with respect to those specimens cured at 45 °C. For specimens activated with 8 mol·kg^{-1}of Na$^+$, the increment on the compressive strength was 77 % and 106 % when cured at 65 °C and 85 °C, respectively. For VA activated using 8 mol·kg^{-1} of Na$^+$, the paste cured at 85 °C developed compressive strength close to 95 MPa.

Adewumi et al. [30] assessed the effect of curing temperature for geopolymeric mortars containing 40 % VA and 60 % limestone powder. Comparing specimens after 7 curing days at 45 °C, an enhancement of 59.5 % and 96.9 % was achieved for specimens cured at 60 °C and 75 °C, respectively. In the same way, Lemougna et al. [26] performed an experimental study using VA from Cameroon for alkali-activated systems with Na$_2$O/SiO$_2$ = 0.25 cured at 40, 70, and 90 °C for 7 days. An increment of 180 % was obtained by comparing specimens cured at 90 °C respect to those cured at 40 °C.

3.3. Influence of curing time on alkali-activated systems

Alkali-activated paste activated with 8 mol·kg^{-1} of Na$^+$ and cured at 65 °C was selected to assess its performance for different curing times. Fourier transform infrared spectroscopy using the attenuated total reflection (FTIR-ATR) technique was used to characterize the band vibration of Si-O for ground VA and alkali-activated pastes. Selected FTIR-ATR spectra between 1200 and 400 cm^{-1} for volcanic ash and alkali-activated pastes are presented in Fig. 10.

It was detected a broad band at 445–467 cm^{-1} indicating the Si-O-

Al^{VI} vibration modes [31], a band at ~535 cm^{-1} representing the ring vibrations of Si-O bonds of the silicate network [32] and a broad hump at 1200–800 cm^{-1} associated with the Si-O-T (being T = Si or Al) asymmetric stretching vibration of silicate structures [33]. A displacement of bands for lower wavenumber values was observed for alkali-activated paste compared to VA, indicating the formation of new compounds, mainly aluminosilicate hydrates [27].

A deconvolution in the infrared spectrum range 1200–800 cm^{-1} was performed to assign and quantify the phases associated with Si-O-T asymmetric stretching vibrations. Using a Gaussian function, the fitting presented an adjusting coefficient (R^2) in the range 0.99858 – 0.99971. Table 2 summarizes the peak position and its relative area with respect to VA. The bands centered at ~970 cm^{-1} and ~874–891 cm^{-1} are attributed to the stretching of Si-O-(M,Me,Fe) or Si-OH, where M is an alkali metal or Me is an alkali-earth metal [34]. These bands did not present a significant variation in their relative area due to the presence of insoluble anorthite and diopside, as could be detected from XRD analysis. Otherwise, the band centered at ~1070–1000 cm^{-1} presented a significant increment in its relative area. It can be assigned to the asymmetric stretching of (Si,Al^{IV})-O-Si in amorphous structures (N-A—S—H gel) [35]. About 50 % of increment is observed for its relative area from 12 h to 72 h of curing, indicating a relevant formation of hydrated products (N-A—S—H gel) in this period.

Compressive strength development of alkali-activated pastes activated with 8 mol·kg^{-1} of Na$^+$ was performed up to 168 h of curing at 65 °C to compare the phase changes observed in FTIR analysis with the macro-property assessed through compressive strength. As can be observed in Fig. 9**b**, there was a significant increase in strength (power function with adjusting parameter R^2 = 0.99) in the first 72 h of curing, achieving about 78 MPa. It represents a 525 % of increment with respect to pastes cured for 12 h (12.47 MPa) which agrees with the high reaction rate of N-A—S—H gel formation observed in the FTIR deconvolution analysis. The positive effect of curing time on compressive strength is reported in several studies: an increment of 281 % was reported for alkali-activated mortars based on vitreous calcium aluminosilicate activated with 10 mol·kg^{-1} NaOH [36].

4. Conclusions

The rapid compressive strength development of alkali-activated systems based on VA is an interesting tool for its application in prefabricated building elements. Although the study was performed using alkali-activated pastes, the feasibility of producing mortars was tested on a laboratory scale, and similar results were obtained. It indicates the great potential of using alkali-activated systems based on VA in reconstructing damaged infrastructures at La Palma Island. Hence, besides providing correct management and consequently valorization of Cumbre Vieja volcanic ash, the feasibility of using this VA in producing alkali-activated systems was demonstrated. Additionally, for the first time, it has been shown the feasibility of using recently erupted volcanic material in developing alkali-activated systems: the non-weathered volcanic ashes are appropriate for this type of system. Long-term studies related to the performance of this alternative cement are in progress and will validate the viability of its use in prefabricated building elements.

CRediT authorship contribution statement

M.M. Tashima: Conceptualization, Methodology, Investigation, Writing – original draft, Writing – review & editing, Supervision, Funding acquisition. **L. Soriano:** Methodology, Investigation, Resources, Writing – original draft, Visualization. **M.V. Borrachero:** Investigation, Resources, Writing – review & editing, Visualization. **J. Monzó:** Methodology, Formal analysis, Investigation, Writing – review & editing, Funding acquisition. **J. Payá:** Conceptualization, Methodology, Formal analysis, Investigation, Resources, Writing – original draft,

Writing – review & editing, Supervision, Project administration, Funding acquisition.

Declaration of Competing Interest

The authors declare the following financial interests/personal relationships which may be considered as potential competing interests: MAURO M. TASHIMA reports financial support was provided by Polytechnic University of Valencia. MAURO M. TASHIMA reports a relationship with Polytechnic University of Valencia that includes: funding grants.

Data availability

Data will be made available on request.

Acknowledgments

References

[1] Gobierno de Canarias, Informe Comité Científico, Islas Canarias, 2021. https://www3.gobiernodecanarias.org/noticias/la-erupcion-de-la-palma-se-declara-finalizada-tras-85-dias-y-8-horas-de-duracion-y-1-219-hectareas-de-coladas/#:~:text=La%20erupci%C3%B3n%20del%20volc%C3%A1n%20que%20este%20s%C3%A1bado%20se%20ha%20dado,la%20lava%20ocup%C3%B3%20480%20hect%C3%A1reas. (accessed September 28, 2022).

[2] M.-A. Longpré, A. Felpeto, Historical volcanism in the Canary Islands; part 1: A review of precursory and eruptive activity, eruption parameter estimates, and implications for hazard assessment, J. Volcanol. Geoth. Res. 419 (2021) 107363.

[3] S.C. Baksh, L.W.S. Finley, Short-circuiting respiration, Science 374 (2021) (1979) 1196–1197, https://doi.org/10.1126/science.abm8098.

[4] S. Barsotti, D. Andronico, A. Neri, P. del Carlo, P.J. Baxter, W.P. Aspinall, T. Hincks, Quantitative assessment of volcanic ash hazards for health and infrastructure at Mt. Etna (Italy) by numerical simulation, J. Volcanol. Geoth. Res. 192 (2010) 85–96, https://doi.org/10.1016/j.jvolgeores.2010.02.011.

[5] G. Cultrone, The use of Mount Etna volcanic ash in the production of bricks with good physical-mechanical performance: Converting a problematic waste product into a resource for the construction industry, Ceram. Int. 48 (2022) 5724–5736, https://doi.org/10.1016/j.ceramint.2021.11.119.

[6] B.F. Houghton, W.A. Cockshell, C.E. Gregg, B.H. Walker, K. Kim, C.M. Tisdale, E. Yamashita, Land, lava, and disaster create a social dilemma after the 2018 eruption of Kīlauea volcano, Nat. Commun. 12 (2021), https://doi.org/10.1038/s41467-021-21455-2.

[7] F.M. (Frederick M. Lea, P.C. Hewlett, M. Liska, Lea's chemistry of cement and concrete, n.d.

[8] Asociación Española de Normalización y Certificación, UNE-EN 197-1 Parte 1: Composición, especificaciones y critérios de conformidad de los cementos comunes (in Spanish), 2011. www.aenor.es.

[9] ASTM International, Standard Specification for Coal Fly Ash and Raw or Calcined Natural Pozzolan for Use in Concrete 1, 2019. https://doi.org/10.1520/C0618-19.

[10] A. Játiva, E. Ruales, M. Etxeberria, Volcanic ash as a sustainable binder material: An extensive review, Materials. 14 (2021) 1–32, https://doi.org/10.3390/ma14051302.

[11] F. Pacheco-Torgal, J.A. Labrincha, C. Leonelli, A. Palomo, P. Chindaprasirt, Handbook of Alkali-activated Cements, Mortars and Concretes, Woodhead Publishing, 2015.

[12] X. Ge, X. Hu, C. Shi, Impact of micro characteristics on the formation of high-strength Class F fly ash-based geopolymers cured at ambient conditions, Constr. Build. Mater. 352 (2022) 129074, https://doi.org/10.1016/J.CONBUILDMAT.2022.129074.

[13] L. Reig, L. Soriano, M.V. Borrachero, J. Monzó, J. Payá, Influence of calcium aluminate cement (CAC) on alkaline activation of red clay brick waste (RCBW), Cem. Concr. Compos. 65 (2016) 177–185.

[14] R. Zhang, Y. Zhang, T. Liu, Q. Wan, D. Zheng, Immobilization of vanadium and nickel in spent fluid catalytic cracking (SFCC) catalysts-based geopolymer, J. Clean. Prod. 332 (2022), 130112, https://doi.org/10.1016/J.JCLEPRO.2021.130112.

[15] J.N.Y. Djobo, A. Elimbi, H.K. Tchakouté, S. Kumar, Reactivity of volcanic ash in alkaline medium, microstructural and strength characteristics of resulting geopolymers under different synthesis conditions, J. Mater. Sci. 51 (2016) 10301–10317, https://doi.org/10.1007/s10853-016-0257-1.

[16] A. Nana, N. Epey, K.C. Rodrique, J.G.N. Deutou, J.N.Y. Djobo, S. Tomé, T. S. Alomayri, J. Ngouné, E. Kamseu, C. Leonelli, Mechanical strength and microstructure of metakaolin/volcanic ash-based geopolymer composites reinforced with reactive silica from rice husk ash (RHA), Materialia (Oxf). 16 (2021) 101083.

[17] K. Nagasawa, Weathering of volcanic ash and other pyroclastic materials, Clays and Clay Minerals of Japan (1978), https://doi.org/10.1016/S0070-4571(08)70683-6.

[18] E. Kuznetsova, R. Motenko, Weathering of volcanic ash in the cryogenic zone of Kamchatka, eastern Russia, Clay Miner. 49 (2014) 195–212, https://doi.org/10.1180/claymin.2014.049.2.04.

[19] H. Hong, Q. Fang, L. Zhao, S. Schoepfer, C. Wang, N. Gong, Z. Li, Z.Q. Chen, Weathering and alteration of volcanic ashes in various depositional settings during the Permian-Triassic transition in South China: Mineralogical, elemental and isotopic approaches, Palaeogeogr. Palaeoclimatol. Palaeoecol. 486 (2017) 46–57, https://doi.org/10.1016/j.palaeo.2016.12.033.

[20] S. Alraddadi, H. Assaedi, Characterization and potential applications of different powder volcanic ash, J King Saud Univ Sci. 32 (2020) 2969–2975, https://doi.org/10.1016/j.jksus.2020.07.019.

[21] B.I. Djon Li Ndjock, A. Elimbi, M. Cyr, Rational utilization of volcanic ashes based on factors affecting their alkaline activation, J. Non Cryst. Solids 463 (2017) 31–39.

[22] J.N. Yankwa Djobo, A. Elimbi, H.K. Tchakouté, S. Kumar, Mechanical activation of volcanic ash for geopolymer synthesis: Effect on reaction kinetics, gel characteristics, physical and mechanical properties, RSC Adv. 6 (2016) 39106–39117, https://doi.org/10.1039/c6ra03667h.

[23] G. Barone, C. Finocchiaro, I. Lancellotti, C. Leonelli, P. Mazzoleni, C. Sgarlata, A. Stroscio, Potentiality of the Use of Pyroclastic Volcanic Residues in the Production of Alkali Activated Material, Waste Biomass Valoriz. 12 (2021) 1075–1094, https://doi.org/10.1007/s12649-020-01004-6.

[24] M.M. Tashima, L. Soriano, J. Monzó, M.V. Borrachero, J. Payá, Novel geopolymeric material cured at room temperature, Adv. Appl. Ceram. 112 (4) (2013) 179–183.

[25] J.N.Y. Djobo, A. Elimbi, H.K. Tchakouté, S. Kumar, Volcanic ash-based geopolymer cements/concretes: the current state of the art and perspectives, Environmental Science and Pollution, Research 24 (2017) 4433–4446, https://doi.org/10.1007/s11356-016-8230-8.

[26] P.N. Lemougna, K.J.D. MacKenzie, U.F.C. Melo, Synthesis and thermal properties of inorganic polymers (geopolymers) for structural and refractory applications from volcanic ash, Ceram. Int. 37 (2011) 3011–3018, https://doi.org/10.1016/j.ceramint.2011.05.002.

[27] H. Takeda, S. Hashimoto, H. Kanie, S. Honda, Y. Iwamoto, Fabrication and characterization of hardened bodies from Japanese volcanic ash using geopolymerization, Ceram. Int. 40 (2014) 4071–4076, https://doi.org/10.1016/J.CERAMINT.2013.08.061.

[28] E. Kamseu, C. Leonelli, D.S. Perera, U.C. Melo, P.N. Lemougna, Investigation of Volcanic Ash Based Geopolymers as Potential Building Materials, InterCeram: International Ceramic Review 58 (2009) 136–140.

[29] M.M. Tashima, L. Soriano, M.V. Borrachero, J. Monzó, C.R. Cheeseman, J. Payá, Alkali activation of vitreous calcium aluminosilicate derived from glass fiber waste, J Sustain Cem Based Mater. 1 (3) (2012) 83–93.

[30] A.A. Adewumi, M.A. Mohd Ariffin, M. Maslehuddin, M.O. Yusuf, M. Ismail, K.A. A. Al-Sodani, Influence of silica modulus and curing temperature on the strength of alkali-activated volcanic ash and limestone powder mortar, Materials. 14 (18) (2021) 5204.

[31] H.K. Tchakouté, S.J.K. Melele, A.T. Djamen, C.R. Kaze, E. Kamseu, C.N.P. Nanseu, C. Leonelli, C.H. Rüscher, Microstructural and mechanical properties of poly(sialate-siloxo) networks obtained using metakaolins from kaolin and halloysite as aluminosilicate sources: A comparative study, Appl. Clay Sci. 186 (2020) 105448.

[32] C. Finocchiaro, G. Barone, P. Mazzoleni, C. Leonelli, A. Gharzouni, S. Rossignol, FT-IR study of early stages of alkali activated materials based on pyroclastic deposits (Mt. Etna, Sicily, Italy) using two different alkaline solutions, Constr Build Mater. 262 (2020). https://doi.org/10.1016/j.conbuildmat.2020.120095.

[33] C.A. Rees, J.L. Provis, G.C. Lukey, J.S.J. van Deventer, In situ ATR-FTIR study of the early stages of fly ash geopolymer gel formation, Langmuir 23 (2007) 9076–9082, https://doi.org/10.1021/la701185g.

[34] W.R. Taylor, Application of infrared spectroscopy to studies of silicate glass structure: Examples from the melilite glasses and the systems Na2O-SiO2 and Na2O-Al2O3-SiO2, 1990.

[35] L.M. Kljajević, S.S. Nenadović, M.T. Nenadović, N.K. Bundaleski, B. Todorović, V. B. Pavlović, Z.L. Rakočević, Structural and chemical properties of thermally treated geopolymer samples, Ceram. Int. 43 (2017) 6700–6708, https://doi.org/10.1016/J.CERAMINT.2017.02.066.

[36] M.M. Tashima, L. Soriano, M.V. Borrachero, J. Monzó, J. Payá, Effect of curing time on microstructure and mechanical strength development of alkali activated binders based on vitreous calcium aluminosilicate (VCAS), Bull. Mater. Sci. 36 (2) (2013) 245–249.